Combined Discrete-Continuum Analysis for Ballasted Rail Tracks

T. Ngo[1,*], B. Indraratna[1] and C. Rujikiatkamjorn[1]

[1]Transport Research Center, School of Civil and Environmental Engineering, Faculty of Engineering and Information Technology, University of Technology Sydney, NSW 2007, Australia
*Email: Trung.Ngo@uts.edu.au (Ph.D, CPEng, M.ASCE)

Abstract. A study on the load-deformation behaviour of railway ballast aggregates subjected to cyclic loadings using a combined discrete-continuum modelling approach is presented. Discrete ballast particles are simulated in the DEM and the continuum-based subgrade is simulated by the FDM. Interface elements are generated to transmit contact forces and displacements between the two domains (i.e. discrete and continuum) whereby the DEM exchanges contact forces to the FDM, and then the FDM transfers the displacement back to the DEM. Distributions of contact forces, coordination number, stress contours on the subgrade and corresponding number of broken bonds (representing ballast breakage) are analysed.

Keywords: ballast, breakage, rail track, DEM, coupled DEM-FDM

1 Introduction

Ballasted railway tracks have an important role in its economy for transporting bulk commodities and freight between ports and major cities as well as moving passengers. The rapidly increasing demand for faster and heavier passenger and heavy haul transport has resulted in an inevitable need for more stable track foundations with lower maintenance costs. Upon repeated passing of trains, ballast grains are degraded and become fouled by the progressive storage of external fine particles within the voids (Selig and Waters 1994, Abadi et al. 2019, Ishikawa et al. 2011, Powrie et al. 2007, Suiker et al. 2005). Fouling causes excessive track settlement and decreases the load-bearing capacity of ballast layers due to a reduction in the shear strength and friction angles of granular layers (Huang et al. 2009, Indraratna et al. 2017, Le Pen and Powrie 2011). Another track problem is where low-lying coastal rail tracks are built on saturated subgrade soils (i.e. water content often approaching the liquid limit) and with continual passage of trains, excess pore pressures and plastic strains accumulate over time, which then leads to an upward ejection of soil slurry to the overlying granular layers (Aursudkij et al. 2009, Al-Qadi et al. 2010, Chen et al. 2018).

2 Combined Discrete-Continuum Modeling

The DEM was initiated earlier by Cundall and Strack (1979) has been growingly adopted for investigating the micro-mechanical behavior of granular aggregates including railway ballast (Cui and O'Sullivan 2006, McDowell and Li 2016, Ngo et al. 2017a). The DEM enables to insightfully investigate the micromechanical features of ballast grains including distributions of contact forces developed among particles, coordination numbers, fabric and contact anisotropy where irregularly-shaped ballast grains and particle breakage can be accurately captured (Tutumluer et al. 2012, Ngo et al. 2014, Jiang et al. 2005, Cui et al. 2019, McDowell et al. 2006, among others). Ballast grain is simulated in DEM where irregular-shaped grains are simulated by bonding of many cylinders together, as illustrated in Figure 1. Micromechanical parameters adopted for ballast grains are determined from calibrating the DEM-based shear stress-displacement responses with those recorded from the laboratory, as given in Table 1.

In this study, an attempt is used to model real ballast particles where clusters of bonded cylinder particles are used to simulate a 2D projection of angular ballast particles, as shown in Figure 1a. Cylinders are bonded together using parallel bonds; and they can be considered as elastic springs having normal stiffness and shear stiffness, uniformly distributed over the contact plane (Fig. 1b). These bonds can carry forces ($\overline{F}_i$) and moment ($\overline{M}_3$). A contact force vector can be described as (Itasca 2016):

$$\overline{F}_i = \overline{F}_i^n + \overline{F}_i^s \tag{1}$$

Force increments over a time-step of Δt are calculated by:

$$\Delta\overline{F}_i^n = \left(-\overline{k}_n A \Delta U_i^n\right) n_i = \left(-2\overline{k}_n \overline{R} t \Delta U_i^n\right) n_i \tag{2}$$

$$\Delta\overline{F}_i^n = \left(-\overline{k}_n A \Delta U_i^n\right) n_i = \left(-2\overline{k}_n \overline{R} t \Delta U_i^n\right) n_i \tag{3}$$

with, $\Delta U_i = V_i \Delta t$

V_i is the shear velocity of particle A relative to particle B at the contact point and is calculated as:

$$V_i = \left(\dot{x}_i^{[B]} - \dot{x}_i^{[A]}\right) t_i \tag{4}$$

Moment increment is computed by:

$$\Delta\overline{M}_3 = -\overline{k}_n I \Delta\theta_3 = -\frac{2}{3}\overline{k}_n \overline{R}^3 t \Delta\theta_3 \tag{5}$$

with, $\Delta\theta_3 = \left(\omega_3^{[B]} - \omega_3^{[A]}\right)\Delta t$; $\overline{k}_n$ and $\overline{k}_s$: normal and shear stiffness of the contact bond, respectively; ΔU_i^n, ΔU_i^s: normal and shear displacement increments; $\omega_3^{[A,B]}$: rotational velocity of particles A, B.

Maximum normal stress (σ_{max}) and shear stress (τ_{max}) are determined by:

$$\sigma_{max} = \frac{-\overline{F}_i^n}{A} + \frac{|\overline{M}_3|}{I}\overline{R} \tag{6}$$

$$\tau_{max} = \frac{\left|\overline{F}_i^s\right|}{A} \tag{7}$$

where, $A = 2\overline{R}t$; $I = \frac{2}{3}\overline{R}^3 t$: are the area and inertia moment of bond cross-section, respectively. If either of these stresses, σ_{max}, τ_{max} is greater than its corresponding bond strength, the parallel bond breaks and this breaking can represent ballast breakage.

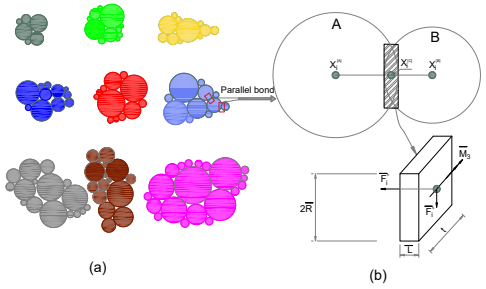

Figure 1. (a) Irregularly-shaped ballast grains; (b) Parallel bond.

A series of large scale track process simulation apparatus tests (TPSA) on ballast were carried out under axle loads of 25 and 35-tonnes subjected to frequencies of f=15 and 20 Hz. More details on the testing apparatus and procedure can be found in Navaratnarajah et al. (2018) and Jayasuriya et al. (2019). The concept of combining the discrete-continuum approach to simulate a TPSA is illustrated in Figure 2, where the model geometry is similar to those conducted in the laboratory.

Given the displacement of ballast in the longitudinal direction (i.e., in the direction of train moving) is very small and could be negligible due to large confinement provided by concrete sleepers and ballast crib, the current combined discrete-continuum analysis (coupled DEM-FDM) is performed in an equivalent plane strain analysis, mimicking typical long and straight tracks. Capping (sub-ballast) and subgrade layers are simulated by the continuum approach using the finite difference method (FDM). Interaction between the discrete ballast grains and continuum capping subgrade are facilitated by interface elements generated at the boundary between DEM and FDM zones, as illustrated in Figure 2 (Ngo et al. 2017b). Principally, the DEM transfers forces and moments to the FDM, and then the FDM transfers displacement back to the DEM domain via interface elements

4 Results and Discussion

Vertical and lateral displacements of ballast are measured during cyclic tests at a given number of load cycle (N). Due to the brevity of this paper, detailed laboratory test results can be found elsewhere (e.g. Indraratna et al. 2013, Jayasuriya et al. 2019, Navaratnarajah et al. 2018); and some of those data are used to calibrate the current DEM analysis. Laboratory test results show that increased axle loads and frequencies result in an increase in ballast vertical settlement and lateral spreading, as expected. Measured test data show that increased axle load from 25-tonne to 35-tonne leads to an increase 29% in settlement and around 9% in lateral displacement of ballast; while increased frequency f to 20 Hz results in an increase 19% and 14% for settlement and horizontal displacement, respectively. In addition, ballast breakage is quantified after each test using BBI (Ballast Breakage Index); and the measured BBI was found to increase from 0.26 to 0.28 when the axle load increase from 25-tonne to 35-tonne.

Table 1 Micromechanical parameters of ballast and USP adopted for DEM simulation

Micro-mechanical parameters used for ballast	Values
Particle density (kg/m3)	2500
Coefficient of friction	0.85
Normal stiffness, k_n (N/m)	4.84×10^8
Shear stiffness, k_s (N/m)	0.968×10^7
Normal stiffness of wall-particle, $k_{n\text{-}wall}$ (N/m)	8.0×10^9
Shear stiffness of wall of wall-particle, $k_{s\text{-}wall}$ (N/m)	4.0×10^9
Damping coefficient	0.7
Parallel bond radius multiplier, r_p	0.5
Parallel bond normal stiffness, k_{np} (kPa/m)	8.68×10^8
Parallel bond shears stiffness, k_{sp} (kPa/m)	4.34×10^8
Parallel bond normal strength, σ_{np} (MPa)	856
Parallel bond shear strength, σ_{sp} (MPa)	428

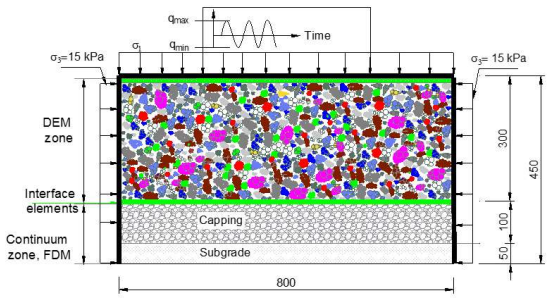

Figure 2. Combined discrete-continuum model for simulating the TPSA

Figure 3 illustrates snapshots of the evolution of bond breakage at varying number of cyclic loads of N=1000 and N=10, 000 cycles, f=15 Hz. The amount of breaking bond and locations of bond breakages are presented in Figures 3a-d. It is seen that an increase in loading, within the first N=1,000 cycles, lots of the bond breakage occur right beneath the sleeper due to high contact forces, as snapshot in the Figures 3a, 3c. An increase in axle loads leads to an increase in the breakage bonds (Figs. 3b, 3d) and the rearranging of broken bonds (i.e. ballast get compacted and restrained from further displacements); and this finding agrees with recent laboratory measurement by Sun et al (2019).

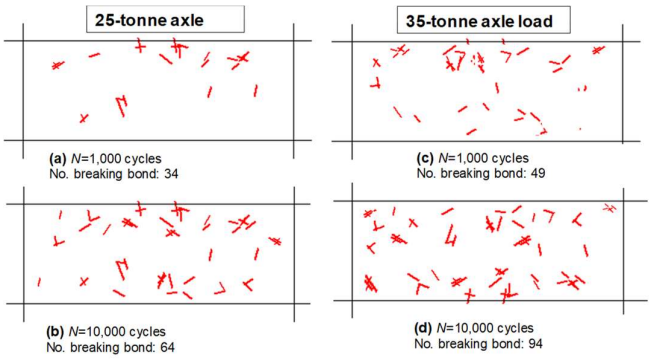

Figure 3. Breaking bonds: (a)-(b): 25-tonne axle load; and (c)-(d): 35-tonne axle load

The shear stress-strain behaviour of granular materials is considered a reflection of its microscopic responses, which is related to coordination number (C_n) (average number of contacts per particle) and the distribution of contacts. Figure 4 shows how the predicted C_n changes when subjected to the application of 25 and 35-tonne axle loads, f=15, 20 Hz. It is predicted that C_n increases initially as the loading cycles increase, followed by a slight reduction towards the end of the simulation. The reduction of C_n may be related to the lateral displacements of the sample and particle breakage.

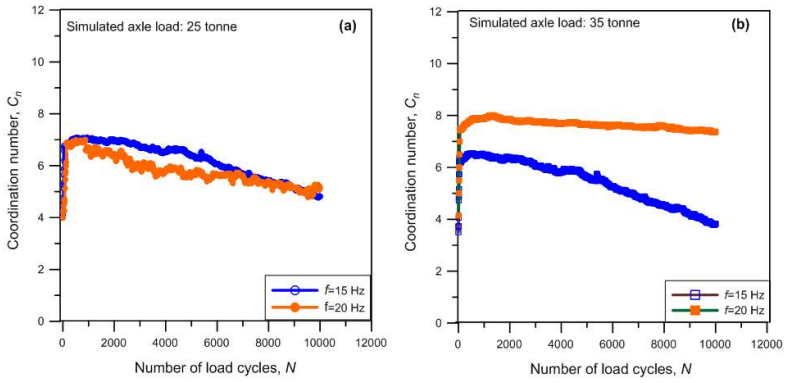

Figure 4. Evolutions of C_n with increased N: (a) 25-tonne axle load; (b) 35-tonne axle load

Figure 5 illustrates the evolutions of contact force distribution in DEM zone and vertical stress contours (FDM zone) at different load cycles of N=1,000 and 10,000 cycles, subjected to 25-tonne (Fig. 5a-b) and 35-tonne axle load (Fig. 5c-d), f=15 Hz. Contact force distributions are plotted at contact points having a thickness proportional to the magnitude of the forces. It is seen that contact forces are distributed non-uniformly, where the maximum contact forces (F_{max}), number of contact force ($N_{c\text{-}force}$) and maximum vertical stresses ($\sigma_{yy\text{-}max}$) change with increased N where there is an increased $N_{c\text{-}force}$ and higher F_{max}, as the ballast gets compacted further and become densified to support the load. An increase in axle loads results in increased F_{max} while increased $N_{c\text{-}force}$, as expected; and this could lead to increased particle breakage, as observed earlier.

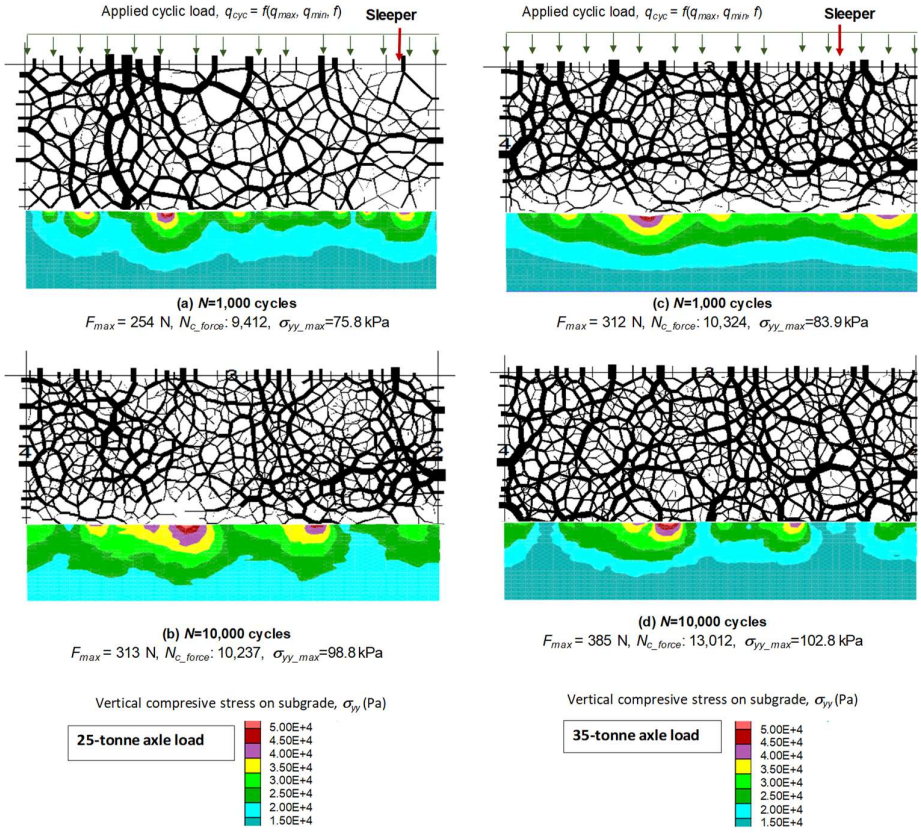

Figure 5. Contact force distribution in DEM region and vertical compressive stress contour on subgrade, subjected to a cyclic axle load of 25 and 35-tonne

8 Conclusions

A coupled discrete-continuum analysis has been carried out to evaluate the breakage of railway ballast when subjected to cyclic train loading in the present study. Four tests were conducted subjected to axle load of 25-tonne and 35-tonne under varying cyclic loading frequencies, f=15 and 20 Hz and test data was used to calibrate and validate the combined DEM-FDM model. The coupling model was then used to predict the number of broken bonds (i.e. representing breakage) and it demonstrated that the broken bonds increased with increased axle loads and frequency. Distributions of contact forces, co-ordination number (C_n) and orientation of contact were also examined; and they showed that the contact forces distributed non-uniformly across the ballast assembly where the maximum contact forces, F_{max} and C_n increased with increased axle loads. Results obtained from this study could provide more insightful micro-mechanical measurements and contact forces distributed across ballast aggregates.

Acknowledgements This research was carried out by the Australian Research Council Industrial Transformation Training Centre for Advanced Technologies in Rail Track Infrastructure (IC170100006) and funded by the Australian Government.

References

Abadi, T., Pen, L.L., Zervos, A. and Powrie, W. (2019). Effect of Sleeper Interventions on Railway Track Performance. J of Geotech and Geoenvir Eng, 145(4), 04019009.

Al-Qadi, I.L., Xie, W., Jonhs, D.L. and Roberts, R. (2010). Development of a time-frequency approach to quantify railroad ballast fouling condition using ultra-wide band ground-penetrating radar data. *International Journal of Pavement Engineering*, 11(4), 269 — 279.

Aursudkij, B., McDowell, G.R. and Collop, A.C. (2009). Cyclic loading of railway ballast under triaxial conditions and in a railway test facility. *Granular Matter*, 11, 391–401.

Chen, W.-B., Yin, J.-H., Feng, W.-Q., Borana, L. and Chen, R.-P. (2018). Accumulated permanent axial strain of a subgrade fill under cyclic high-speed railway loading. *International Journal of Geomechanics*, 18(5), 04018018.

Cui, L. and O'Sullivan, C. (2006). Exploring the macro- and micro-scale response of an idealised granular material in the direct shear apparatus. *Geotechnique*, 56(7), 455-468.

Cui, L., Bhattacharya, S., Nikitas, G. and Bhat, A. (2019). Macro- and micro-mechanics of granular soil in asymmetric cyclic loadings encountered by offshore wind turbine foundations. *Granular Matter*, 21(3), 73.

Cundall, and Strack, O. (1979). A discrete numerical model for granular assemblies. *Geotechnique*, 29(1), 47-65.

Huang, H., Tutumluer, E. and Dombrow, W. (2009). Laboratory characterisation of fouled railroad ballast behavior. *Transportation Research Record*: No. 2117, Washington, DC.

Indraratna, B., Ngo, N.T. and Rujikiatkamjorn, C. (2013). Deformation of coal fouled ballast stabilized with geogrid under cyclic load. *Journal of Geotechnical and Geoenvironmental Engineering*, 139(8), 1275-1289.

Ishikawa, T., Sekine, E. and Miura, S. (2011). Cyclic deformation of granular material subjected to moving-wheel loads. *Canadian Geotechnical Journal*, 48(5), 691-703.

Indraratna, Nimbalkar, Ngo, T. Neville. (2016). Performance improvement of rail track substructure using artificial inclusions – Experimental and numerical studies. *Transportation Geotechnics*, 8, 69-85.

Itasca (2016). Particle flow code in three dimensions (PFC3D). . Itasca Consulting Group, Inc.,

Jiang, M.J., Yu, H.S. and Harris, D. (2005). A novel discrete model for granular material incorporating rolling resistance. *Computers and Geotechnics*, 32, 340–357.

Jayasuriya, C., Indraratna, B. and Ngo, T.N. (2019). Experimental study to examine the role of under sleeper pads for improved performance of ballast under cyclic loading. *Transportation Geotechnics*, 19, 61-73.

Le Pen, and Powrie, W. (2011). Contribution of Base, Crib, and Shoulder Ballast to the Lateral Sliding Resistance of Railway Track. *Journal of Rail and Rapid Transit*, 225(2), 113-128.

McDowell, Harireche, Konietzky, H., Brown, Thom (2006). Discrete element modelling of geogrid-reinforced aggregates. *Geotechnical Engineering* 159(1), 35-48.

McDowell, G.R. and Li, H. (2016). Discrete element modelling of scaled railway ballast under triaxial conditions. *Granular Matter*, 18(3), 66.

Navaratnarajah, S.K., Indraratna, B. and Ngo, N.T. (2018). Influence of under sleeper pads on ballast behavior under cyclic loading: experimental and numerical studies. *Journal of Geotechnical and Geoenvironmental Engineering*, 144(9), 04018068.

Ngo, N.T., Indraratna, B. and Rujikiatkamjorn, C. (2014). DEM simulation of the behaviour of geogrid stabilised ballast fouled with coal. *Computers and Geotechnics*, 55, pp: 224-231.

Ngo,T., Indraratna and Rujikiatkamjorn. (2017a). A study of the geogrid–subballast interface via experimental evaluation and discrete element modelling. *Granu. Matter*, 19(3), 51-16.

Ngo, N.T., Indraratna, B. and Rujikiatkamjorn, C. (2017b). Simulation Ballasted Track Behavior: Numerical Treatment and Field Application. Int J Geomech, 17(6), 04016130.

Powrie, W., Yang, L.A. and Clayton, C.R.I. (2007). Stress changes in the ground below ballasted railway track during train passage. *Journal of Rail and Rapid Transit*, 247-261.

Selig, E.T. and Waters. (1994). Track geotechnology and substructure management, Telford.

Sun, Q., Indraratna, B. and Ngo, N.T. (2019). Effect of increase in load and frequency on the resilience of railway ballast. *Géotechnique,* 69(9), 833–840.

Suiker, J., Selig, T. and Frenkel, R. (2005). Static and cyclic triaxial testing of ballast and subballast. J*ournal of Geotechnical and Geoenvironmental Engineering, ASCE* 131(6), 771–782.

Tutumluer, E., Huang, H. and Bian, X. (2012). Geogrid-aggregate interlock mechanism investigated through aggregate imaging-based discrete element modeling approach. *Int J Geomech*, 12(4), 391-398.